JACS
JOURNAL OF THE AMERICAN CHEMICAL SOCIETY

Article

pubs.acs.org/JACS

Unleashing the Quadratic Nonlinear Optical Responses of Graphene by Confining White-Graphene (*h*-BN) Sections in Its Framework

Panaghiotis Karamanis,* Nicolás Otero, and Claude Pouchan

Equipe de Chimie Théorique, ECP Institut des Sciences Analytiques et de Physico-chimie pour l'Environnement et les Matériaux (IPREM) UMR 5254, Hélioparc Pau Pyrénées 2 avenue du Président Angot, 64053 Pau Cedex 09, France

Supporting Information

ABSTRACT: In an attempt to diversify the options in designing graphene-based systems bearing large second order nonlinear optical (NLO) responses of octupolar and/or dipolar character, the subject of the quadratic NLO properties of hybrid boron nitride (BN) graphene flakes is opened up. State of the art ab initio and density functional theory methods applied on a toolbox of book-text octupolar and arbitrary dipolar planar hybrid *h*-BN−graphene nanosized systems reveal that by confining finite *h*-BN sections in the internal network of graphene, the capacity of the π-electron network of graphene species in delivering giant second order NLO responses could be fully exploited. Configuration interaction (CIS) and time-dependent density functional (TD) computations, within the sum-overstate (SOS) perturbational approach, expose that the prevailing (hyper)polarization mechanism, lying under the sizable computed octupolar hyperpolarizabilities, is fueled by alternating positive and negative atomic charges located in the internal part of the hybrid flakes, and more precisely at the BN/graphene intersections. This type of charge transfer mechanism distinguishes, in fact, the elemental graphene dipoles/octupoles we report here from other conventional NLO dipoles or octupoles. More interestingly, it is shown that by controlling the shape, size, and covering area of the *h*-BN domain (or domains), one can effectively regulate "à volonté" both the magnitudes and types of the second order NLO responses switching from dipolar to octupolar and vice versa. Especially in the context of the latter class of NLO properties, this communication brings into surface novel, graphene-based, octupolar planar or quasiplanar motifs. The take home message of this communication is summarized as follows: When the right BN segment is incorporated in the right section of the right graphene flake, systems of giant quadratic NLO octupolar and/or dipolar responses may emerge.

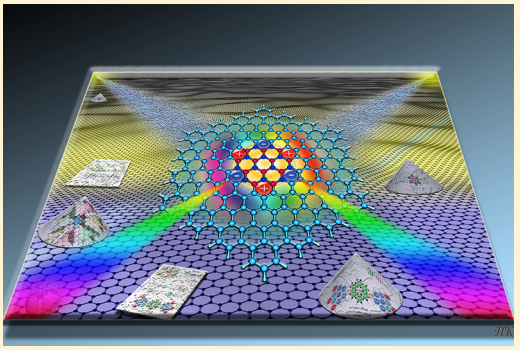

INTRODUCTION

The clear scientific hypothesis that the extended 2D-π-electron network of graphene-based[1] systems could be largely displaced (hyperpolarized) under the influence of strong external electric fields delivering large nonlinear optical responses (NLO) has been proven correct both in theory and practice. As a result, extraordinary NLO graphene features[2] such as saturable absorption, ultrafast NLO responses,[3] high quadratic electro-optic effect (Kerr effect), coherent ultrabroadband nonlinear optical response, giant optical limiting effects, and so on,[4−7] have been already brought to surface. It is believed[8] that such NLO features,[9] if combined with the distinctive qualities of graphenes, may eventually deliver ground-breaking NLO devices within which the substantial potential of light could be fully exploited, boosting up the performance of a vast assortment of existing technologies.[10]

Among the various NLO processes studied so far in graphene, those related to the third order/cubic NLO phenomena have attracted most of the attention. On the contrary, for the equally important second order/quadric responses, also related to crucial technological applications,[11] the up-to-date reported work is rather limited. This should not be surprising since ideal 2D graphene is centrosymmetric, whereas the second order NLO properties of isolated noncentrosymmetric pristine graphene finite sections in most of the cases are found negligible. Therefore, several designing strategies have been exploited aiming at setting in motion the second order NLO responses of graphene. These efforts have been based mostly on gained knowledge[12] from earlier studies on organic/organometallic molecules and polymers. As a result, edge-functionalized graphene with foreign electron donor/acceptor units, or even metals, have occupied so far most of the interest about their quadratic NLO properties.[13−16]

In the current proof-of-concept article an alternative route is proposed. Instead of functionalizing graphene edges, it will be shown that by modifying its internal network one may exploit more efficiently the existing capacity of its π-electron network species in favor of the second order NLO responses. More specifically, it will be demonstrated that upon confinement of boron nitride finite sections (*h*-BN or white graphene) in the framework of pristine graphene flakes, not only their first order

Received: March 20, 2014
Published: April 29, 2014

   dx.doi.org/10.1021/ja502631w | *J. Am. Chem. Soc.* 2014, 136, 7464−7473

NLO responses are switched-on, but also systems of exceptionally high NLO activity at the static limit may emerge. More interestingly, it will be proven that depending on the shape, size, and covering area of the *h*-BN patch, one can efficiently tune both the magnitude and type of the second order NLO responses switching from dipolar to octupolar[17] systems. Especially the latter type of molecular motifs, which represent a classical paradigm of purpose-oriented molecular engineering in the NLO realm, are considered of primary importance in the research of efficient NLO materials.[17,18]

Our interest in opening up the subject of the second order NLO responses in such hybrid systems has been fueled by recent advances in synthesis and characterization of ground breaking two-dimensional white-graphene/graphene hybrids.[19] Advanced systems of this type are currently grown in the lab as a part of several efforts in opening and controlling the band gap[20] of graphene via the so-called negative-type (nitrogen) positive-type (boron) doping. The fruits of these initial endeavors have already proven very promising. For instance, Chang et al.[21] recently reported a gap opening of 600 meV that is attributed to $\pi-\pi^*$ band gap opening of graphene owing to the isoelectronic BN domains embedded in the framework of graphene. In another work Bepete et al.[22] managed to control the incorporation of small *h*-BN sections of the size of coronene in graphene, via chemical vapor deposition (CVD). Also, independent theoretical studies suggest that the separation of the occupied and unoccupied bands in graphene could be tuned by controlling the distance between the embedded *h*-BN sections.[20]

RESULTS AND DISCUSSION

To establish the above-described proof-of-concept we choose to start from the ideal molecular hybrid planar BN−graphene armchair[23] flakes of increasing size shown in Figure 1. Among the four hybrids depicted, one can distinguish *h*-$B_{12}N_{12}$−C_{222}, which in its pristine molecular graphene form as $C_{222}H_{42}$ can be experimentally obtained from cyclodehydrogenation of polyphenylenes.[24] By introducing precisely at the center of these hexagonal pristine-graphene sections of D_{6h} symmetry, a hexagonal boron nitride patch of the size of coronene, hybrid systems belonging to the D_{3h} point group are obtained. This is the most attractive feature of these *h*-$B_{12}N_{12}$−graphene architectures since the latter trigonal symmetry, which is also the symmetry of the free $B_{12}N_{12}$, is the octupolar-archetype in two dimensions.[17]

Atomic charges, obtained with the fractional occupation Hirshfeld iterative (FOHI) method as developed by Van Alsenoy and co-workers,[25] also presented in Figure 1, expose a flawless octupolar distribution imposed into two dimensions by alternating negative and positive charges localized at each peak of the *h*-$B_{12}N_{12}$ section. These charges correspond to three pairs of B and N atoms, respectively, located at the graphene−BN intersection. A detailed analysis of the corresponding 2-center (2DI) delocalization indices,[26,27] representing the electron population shared between all possible atom pairs of this flake, suggests that the alternating +/− charges shown in Figure 1 are connected to swapping covalent bonding strengths occurring at the periphery of the BN patch. For instance all N−C of *h*-$B_{12}N_{12}$−C_{222} bonds are found 1.4 times "more covalent" (or "less ionic") than the corresponding B−C bonds (δ_2(N−C) = 1.4 × δ_2(B−C)). This result verifies what is implied by the relative FOHI charges between B, N, and C atoms about the existing bonding patterns in graphene−BN intersection.

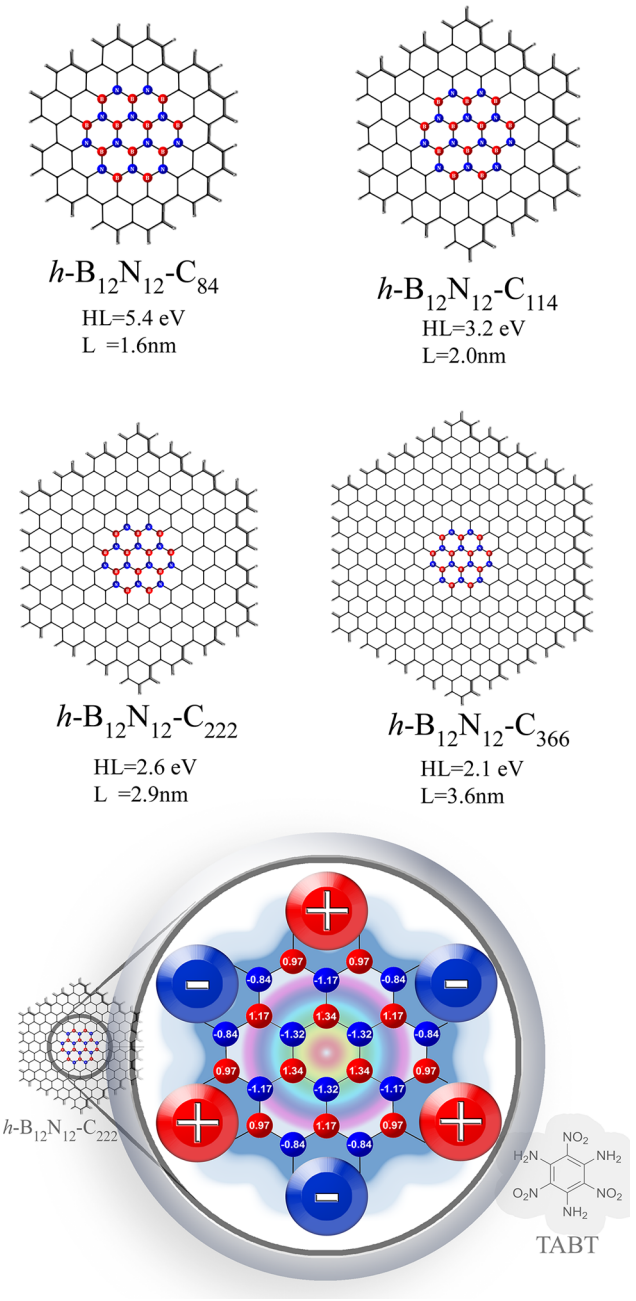

Figure 1. Structures of hexagonal armchair *h*-$B_{12}N_{12}$−graphene hydrogen passivated flakes of D_{3h} symmetry optimized with the B3LYP functional (*h*-$B_{12}N_{12}$−C_{84}, −C_{114}: B3LYP/6-31G(d), and *h*-$B_{12}N_{12}$−C_{222}, −C_{366}: B3LYP/6-31G) and $FOHI_{[B3LYP/6-31G(d)]}$ atomic charges of the central $B_{12}N_{12}$ segment of *h*-$B_{12}N_{12}$−C_{222}. All geometries up to C_{114} correspond to true minima characterized by all real harmonic frequencies. The abbreviations L and HL stand for the diameter of each flake and their respective HOMO−$LUMO_{[CAM-B3LYP/6-31G(d)]}$ gaps, respectively. The ground state electronic structures of all systems are closed-shell singlets with a singlet−triplet $gap_{[CAM-B3LYP/6-31G(d)]}$ varying from 74 kcal/mol for the smallest flake to 19 kcal/mol for the largest, as computed at the CAM-B3LYP/6-31G(d) level of theory.

From an alternative point of view, the octupolar charge distribution observed in the *h*-$B_{12}N_{12}$ section shares similar basic characteristics with one the of the first ever octupoles synthesized and studied for its NLO activity. That is 2,4,6-triamino-1,3,5-trinitrobenzene widely known as TATB. TATB

dx.doi.org/10.1021/ja502631w | J. Am. Chem. Soc. 2014, 136, 7464−7473

Table 1. Modulus of the First Hyperpolarizabity $\|\beta\|$[a] and the Square Roots of the Experimental Observables $\langle\beta_{zzz}^2\rangle$[b] and $\langle\beta_{HRS}^2\rangle$ at the Static Limit (Off-Resonance) Computed at Various Levels of Theory[c]

	$\|\beta\|$	$(\langle\beta^2_{HRS}\rangle)^{1/2}$	$(\langle\beta^2_{zzz}\rangle)^{1/2}$
***h*-$B_{12}N_{12}H_{24}$**	× 10^3	× 10^3	× 10^3
HF	1.0	0.31	0.24
MP2	1.5	0.46	0.36
CAM-B3LYP[d]	1.3	0.41	0.32
LC-BLYP[e]	1.3	0.39	0.30
BH&HLYP[f]	1.2	0.38	0.30
B2PLYP[g]	1.4	0.45	0.35
***h*-$B_{12}N_{12}$–C_{84}**	× 10^3	× 10^3	× 10^3
HF	6.2	1.9	1.5
CAM-B3LYP	7.3	2.2	1.7
LC-BLYP	6.6	2.0	1.6
BH&HLYP	7.1	2.2	1.7
B2PLYP	8.0	2.5	1.9
***h*-$B_{12}N_{12}$–C_{114}**	× 10^4	× 10^4	× 10^4
HF	3.1	0.9	0.7
CAM-B3LYP	5.7	1.8	1.4
LC-BLYP	4.5	1.4	1.1
BH&HLYP	6.0	1.9	1.4
B2PLYP	7.5	2.3	1.8
***h*-$B_{12}N_{12}$–C_{222}**	× 10^5	× 10^4	× 10^4
HF	1.0	3.2	2.5
CAM-B3LYP	1.5	4.8	3.7
LC-BLYP	1.3	4.0	3.1
BH&HLYP	1.6	5.0	3.9
***h*-$B_{12}N_{12}$–C_{366}**	× 10^5	× 10^5	× 10^4
HF	2.8	0.9	6.8
CAM-B3LYP	3.7	1.1	8.8
LC-BLYP	3.2	1.0	7.7
BH&HLYP	3.9	1.2	9.3

[a] $\|\beta\| = (\Sigma_{i,j,k}\beta_{ijk}^2)^{1/2} = [\beta_{xxx}^2 + \beta_{yyy}^2 + \beta_{zzz}^2 + 3(\beta_{xyy}^2 + \beta_{xzz}^2 + \beta_{yxx}^2 + \beta_{yzz}^2 + \beta_{zxx}^2 + \beta_{zyy}^2) + 6\beta_{xyz}^2]^{1/2}$. Within the D_{3h} octupolar point group and for the orientation considered here, there is only one active independent second order tensorial component, that is β_{yyy} (= $-\beta_{xyy}$). As a result, we have $\|\beta\| = 2\beta_{yyy}$. [b] $\langle\beta_{zzz}^2\rangle$ and $\langle\beta_{HRS}^2\rangle$ connect the molecular with the laboratory coordinates in Hyper-Rayleigh Scattering (HRS) experiments which are suitable for measurements in octupolar species. For systems of D_{3h} symmetry $\langle\beta_{zzz}^2\rangle = 24/105\beta_{zzz}^2$ and $\langle\beta_{HRS}^2\rangle = 16/105\beta_{zzz}^2$. [c] Levels of theory include Hartee–Fock, second order Møller–Plesset perturbation theory (MP2), Görling–Levy perturbation theory-based functional B2PLYP,[33] and three DFT functionals of different construction. All calculations have been performed with the 6-31G(d) (a careful and systematic basis set effect study is given as Supporting Information together with a more detailed discussion about the performance of the DFT methods we considered in this work) basis set and the GAUSSIAN 09[34] suite of programs. MP2 and B2PLYP hyperpolarizabilities have been computed within the finite field scheme,[35] while HF and DFT values correspond to analytic hyperpolarizability computations. [d] CAM-B3LYP, the long-range corrected version of B3LYP that uses the Coulomb-attenuating method, (CAM). [e] The long-range corrected LC-BLYP with the default range separation parameter (μ = 0.47). BLYP is the Becke's 1988 exchange functional, combined with the Lee, Yang, and Parr. [f] The "half and half functional" BH&HLYP, as implemented in GAUSSIAN 09. [g] This semiempirical functional was proposed by Grimme and it is based on a mixing of standard generalized gradient approximations for exchange by Becke and for correlation by Lee, Yang, and Parr with Hartree–Fock exchange and a perturbative second order correlation part that is obtained from the Kohn–Sham orbitals and eigenvalues.

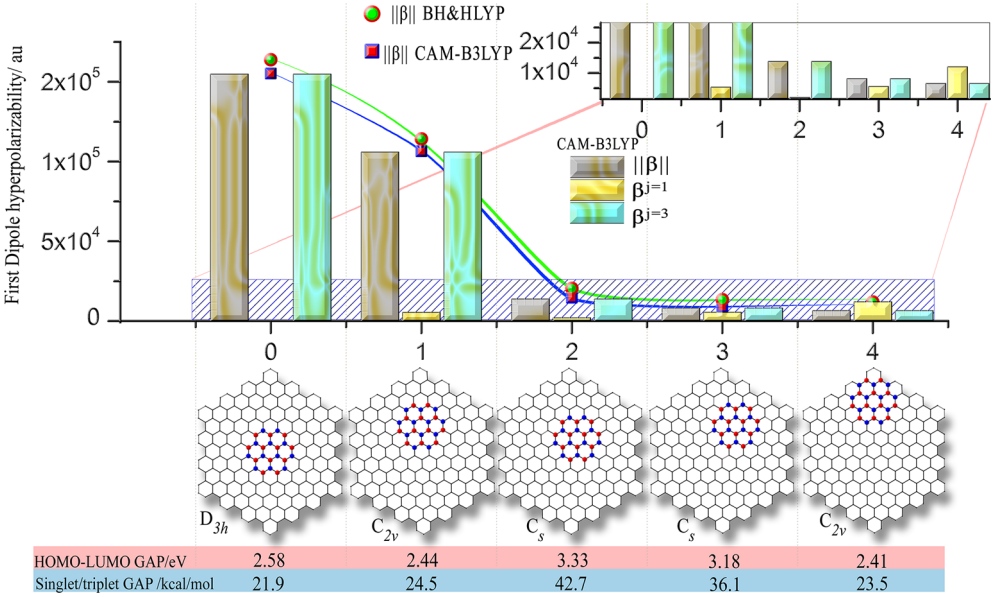

Figure 2. $\|\beta\|$ dependence on the covering area of $B_{12}N_{12}$ in the framework of C_{222} graphene flake at CAM-B3LYP, BH&HLYP/6-31G(d) level of theory. In this figure we also show the values of the moduli of the two irreducible spherical tensors used to decompose the dipolar ($\beta^{J=1}$) and octupolar contributions ($\beta^{J=3}$) on the β tensor as $\beta = \beta^{J=1} \oplus \beta^{J=3}$.[17] All geometries have been optimized at the B3LYP/6-31G level. The ground state electronic structures of all systems are singlets with singlet–triplet$_{[CAM\text{-}B3LYP/6\text{-}31G(d)]}$ gaps varying from 42.6 to 23.5 kcal/mol and HOMO–LUMO$_{[CAM\text{-}B3LYP/6\text{-}31G(d)]}$ gaps from 2.58 to 3.33 eV.

dx.doi.org/10.1021/ja502631w | J. Am. Chem. Soc. 2014, 136, 7464–7473

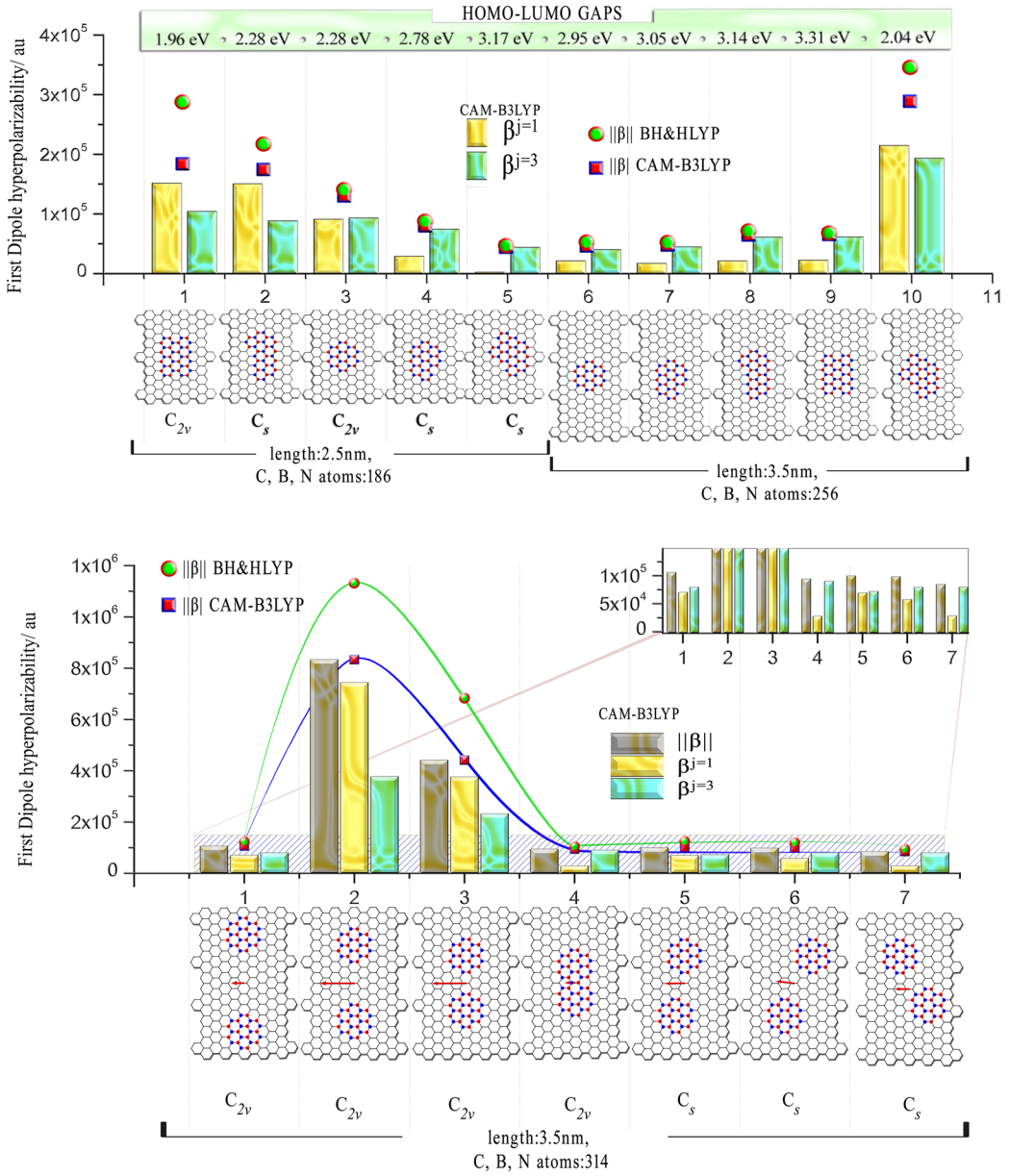

Figure 3. Structure–hyperpolarizability correlations among different hybrid *h*-B_nN_n–graphene systems bearing one (top) or two *h*-B_nN_n (bottom) sections of varying size and shape in their framework. Note that the symmetry of each hybrid BN–graphene system is defined by the symmetry and the covering area of the BN section in the framework of these molecular graphenes. The geometries of all systems have been optimized at the B3LYP/6-31G level. The arrows shown in each hybrid system at the bottom represent the respective ground state dipole moments (size and direction). The HOMO–LUMO gaps corresponding to *h*-B_nN_n–graphene systems bearing one section of varying size and shape in their framework have been computed at the CAM-B3LYP/6-31G(d) level of theory. All models are hydrogen-passivated.

has been exhaustively studied for its octupolar NLO properties[17] as the trigonal analogue of the dipolar prototype of para-nitroniline widely referred as pNa. The main difference here is that $B_{12}N_{12}$, instead of standing as an independent unit, is confined in the heart of a well-defined 0D graphene host. Hence, one can reasonably consider the model systems presented in Figure 1 as book-text cases of planar octupolar graphene-based systems.

D_{3h} symmetry point group constrains require from the patched flakes illustrated in Figure 1 to carry vanishing dipole moments, vanishing dipolar contributions to the first hyperpolarizability tensor at the static limit, but active octupolar first order NLO responses.[17] What cannot be predicted by symmetry is the size of the expected NLO activity. For this reason, we performed extensive hyperpolarizability computations at various levels of theory, the most representative fraction of which is presented in Table 1. The main observable in the values listed in this table is of course the giant octupolar NLO second order responses predicted for the larger in size species. See for instance the evolution of $\|\beta\|$ with the flake size. As we go from *h*-$B_{12}N_{12}$–C_{84} to C_{366} the hyperpolarizability magnitudes outweigh the barrier of 10^5 au,[12,28] and this holds for all methods we considered here. A similar trend is observed for both $\langle\beta_{zzz}^2\rangle$ and $\langle\beta_{HRS}^2\rangle$. What's interesting in these results is the fact that the obtained responses are by far larger in the hybrid systems than in their constituent parts. Compare for instance the hyperpolarizabilities of the patched flakes with those of the free $B_{12}N_{12}H_{24}$, presented in Table 1. It is more

dx.doi.org/10.1021/ja502631w | J. Am. Chem. Soc. 2014, 136, 7464–7473

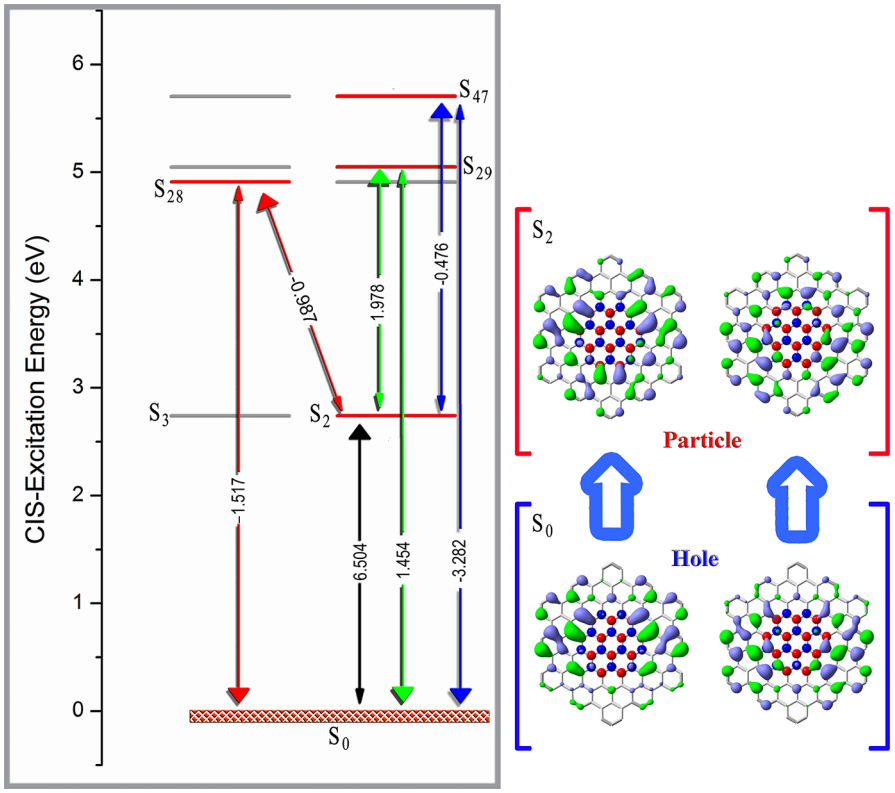

Figure 4. (left) Configuration interaction singlets (CIS/6-31G(d)) depiction of the dominant excitation paths ($S_0 \rightleftarrows S_2 \rightleftarrows S_m \rightleftarrows S_0$ m = 28, 29, and 47) contributing the most on the hyperpolarizability of h-$B_{12}N_{12}$−C_{114} along the y-axis (β_{yyy}) (S_0 is the ground state). Numbers attributed to each arrow represent ground to excited state and excited to excited state transition dipoles in atomic units. For purely octupolar molecules the later tensorial components should be proportional to the sum-overstates (SOS) octupolar term $[\Sigma_n\Sigma_{m\neq n}(\mu^y_{0n}\mu^y_{nm}\mu^y_{m0})(E_{0n}E_{0m})^{-1}]$. Note that the CIS outcomes obey without the slightest deviation the symmetry rules holding in octupolar configurations of D_{3h} symmetry. For instance, the dipole moment of the ground state $S_0\vec{\mu}_{S0}$ is null, while the dipole moments of the degenerated states S_2 and S_3, are of equal magnitude (1.900 au) but of opposite sign. The same holds for the transition moments μ^y_{02} and μ^x_{03} corresponding to the electronic transitions $S_0 \rightarrow S_2$ (μ^y_{02} = 6.504 au) and $S_0 \rightarrow S_3$ (μ^x_{02} = −6.504 au), respectively, since $\vec{\mu}_{02} \perp \vec{\mu}_{03}$. (right) Natural transition orbital pairs for the transition $S_0 \rightarrow S_3$ derived from the CIS/6-31G(d) density matrix.

than evident that $B_{12}N_{12}H_{24}$ is by far less hyperpolarizable than each of the hybrid graphene flakes listed in the same table.

The hyperpolarizability magnitudes of the values listed in Table 1 are found comparable to those of propeller-shaped conjugated organic octupolar molecules previously studied by Brunel et al.[29−31] These authors reported $\|\beta\|$ values near the limit of 1×10^5 au, which is in the range of our outcomes in the case of h-$B_{12}N_{12}$−C_{222}. On the other hand, those obtained for h-$B_{12}N_{12}$−C_{366} are found 3 times larger. For the latter system the magnitude of the computed $(\langle\beta^2_{HRS}\rangle)^{1/2}$ of 1.2×10^5 comes within reach of one of the largest experimental off-resonance hyperpolarizabilities ever reported for an octupolar molecule. The respective intervalence band $(\langle\beta^2_{HRS}\rangle_{1907nm})^{1/2}$ value of 6.6 $\times 10^5$ au (5750×10^{-30} esu) recently reported by Ayhan et al.,[18] belongs to an actinide complex (Bis(phtalocyaninato) lutetium III) of T_d symmetry. The latter symmetry is the analogue octupolar-archetype in a three-dimensional space. On the basis of the scaling of the first hyperpolarizabilities shown in Table 1 with flake size, one could guesstimate that by increasing the size of these flakes, static-hyperpolarizability sizes as substantial as those reported by Ayhan et al. most likely should be obtained.[32]

Figure 2 depicts the evolution of $\|\beta\|$ in several isomers of h-$B_{12}N_{12}$−C_{222} in which the $B_{12}N_{12}$ section occupies different hexagonal segments of the flake. It is more than evident that the covering area of the BN section, which in principle defines the symmetry of each hybrid system, not only is related to the obtained octupolar/dipolar hyperpolarizability types, but also is related to their sizable magnitudes. Interestingly, the maximum NLO response is delivered only when the BN patch is placed precisely at the center of the flake (D_{3h}, $\|\beta^{J=1}\| = 0$). Contrarily, a severe hyperpolarizability decrease is experienced when the BN patch moves toward the flake-edges. What makes these results more challenging to rationalize is the fact that the evidenced hyperpolarizability variations show no obvious connection with the respective HOMO−LUMO gaps.

The strong influence of the structure on the first hyperpolarizability in such hybrid flakes magnitudes is totally verified by the additional results summarized in Figure 3. In brief, in Figure 3 (top) hyperpolarizability results corresponding to two rectangular hybrid BN−graphene flakes 2.5 and 3.5 nm in length built from 186, 256 B and N atoms, are given. It is obvious that depending on the shape or size of the BN-patches,[36] large variations in the computed hyperpolarizability sizes are obtained reflecting as well on the computed $\beta^{J=1}/\beta^{J=3}$ relative sizes. What is intriguing here is that $\|\beta\|$ does not scale with the total flake size in a uniform manner. See, for instance, the differences in hyperpolarizability between hybrid flakes **#1** and **#9**, which share the same symmetry (C_{2v}) and the same $B_{18}N_{18}$ confined ribbon at their center. Hybrid flake **#1**, although 1 nm shorter, is found about two times more hyperpolarizable than hybrid flake **#9**. What's more, the dipolar

dx.doi.org/10.1021/ja502631w | J. Am. Chem. Soc. 2014, 136, 7464−7473

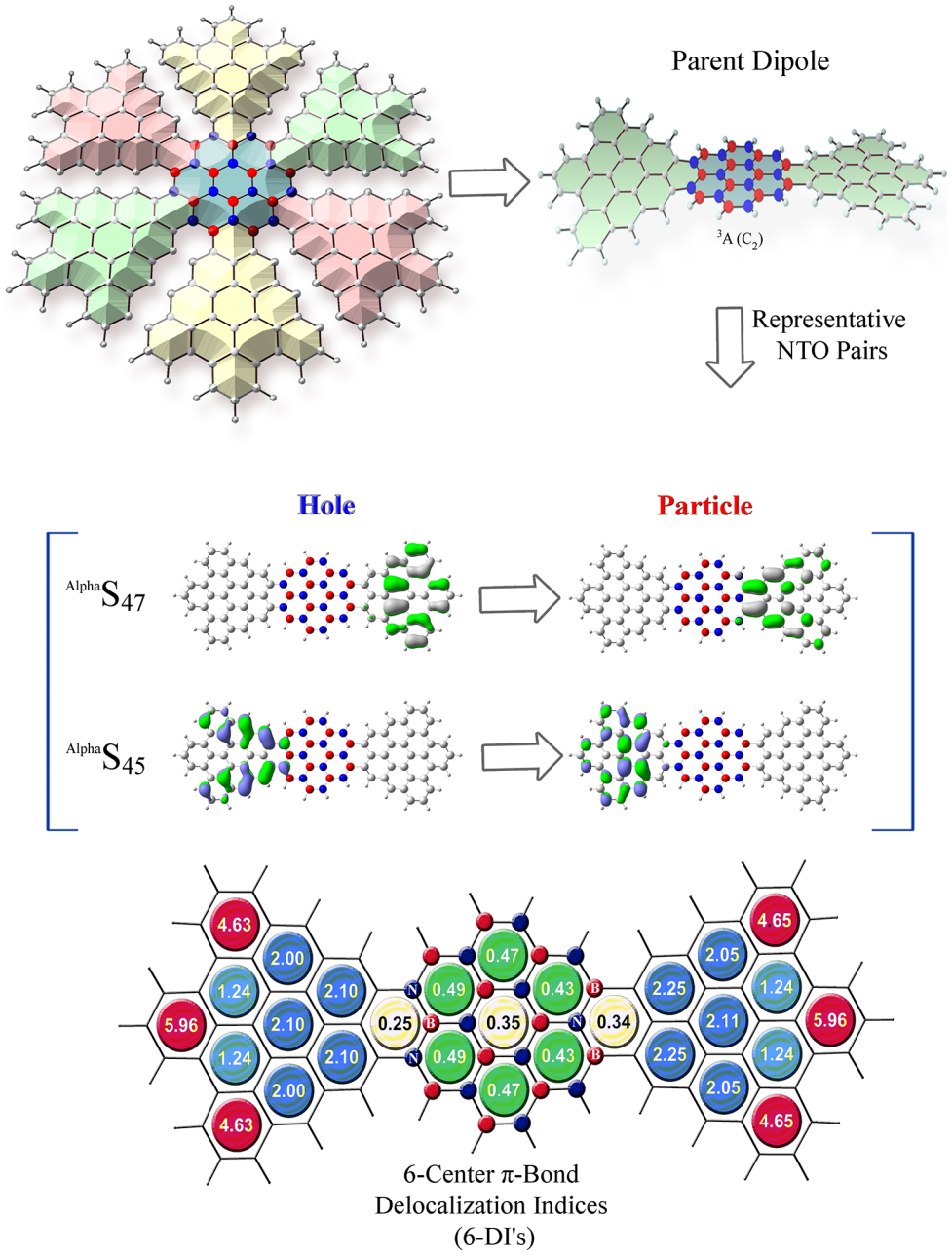

Figure 5. (top) Segmentation of *h*-$B_{12}N_{12}$−C_{222} into three equivalent dipoles. The ground electronic states of each dipole is a triplet, while each of these elementary fragments bear a slightly twisted geometry of the C_2 symmetry. The obtained $\beta^{J=1}/\beta^{J=3}$ ratios, representing the relative dipolar/octupolar contribution, mirror the strong dipolar character of their first hyperpolarizabilities. For instance, at CAM-UB3LYP/6-31G(d) level, $\|\beta\|$ amounts to 8.0×10^3 au, while at the same level of theory $\beta^{J=1}/\beta^{J=3} = 1.7$. (middle) Representative natural transition orbital pairs corresponding to the electronic excitations $S_0 \rightarrow S_{45}$ and $S_0 \rightarrow S_{47}$ derived from the TDA-UCAM-B3LYP/6-31G(d) density matrix. (bottom) FOHI *n*-center π-bond delocalization indices for $n = 6$ (π-6-DIs) accounting for the 95% of the total *n*-DIs for highly delocalized systems when $n > 4$. π-6-DIs values are given in au multiplied with 10^3. These numbers clearly show that delocalization in the carbon wings is notably larger than in the BN section (maximal difference ($\Delta_6^\pi = 4.7 \times 10^{-4}$ au) of 2.6 times less than the least aromatic ring in the first group ($\Delta_6^\pi = 1.2 \times 10^{-3}$ au).

contributions in flake **#1** are more pronounced than the octupolar ones, whereas the opposite picture holds in hybrid flake **#9**. In striking contrast, a reverse trend is evidenced in hybrid flakes **#5** and **#10**. Obviously, the complexity of the problem increases with the size of the systems indicating that such motifs may offer considerable flexibility in optimizing their NLO properties by controlling the relative BN/graphene sizes. This last deduction is confirmed by the computational outcomes summarized in Figure 3 (bottom). There, it is seen that in graphene flakes bearing more than one BN section in their structure, both the hyperpolarizability magnitudes and the relative octupolar/dipolar character of their NLO responses can be vastly maximized by controlling the distance and relative position between the BN sections. See, for instance, the giant hyperpolarizability value obtained for hybrid flake **#2** reaching an order of 10^6 au.

The source of the unorthodox hyperpolarizability variations observed in the rectangular hybrids shown in Figure 3 with respect to their size lies in the excitation energies as implied by the HOMO and LUMO gaps shown in Figure 3 (top). At the

dx.doi.org/10.1021/ja502631w | *J. Am. Chem. Soc.* 2014, 136, 7464−7473

CAM-B3LYP/6-31G(d) level of theory flake #**1** bears a gap of 1.96 eV, while in flake #**9** the corresponding energy separation amounts to 3.3 eV. The same holds for flake #**5** (HL = 3.17 eV) and flake #**10** (HL = 2.04 eV). The respective differences are large enough to justify up to a great extent the observed hyperpolarizability−magnitude variations. In the same manner hybrid flake #**2** shown in Figure 3 (bottom) proves more hyperpolarizable than flake #**3** of the same family. The first hybrid system features a HOMO−LUMO gap of 1.43 eV, while in the latter the respective gap is found about 0.33 eV wider.

So far, we have seen that in *h*-B_nN_n−graphene hybrid planar systems the sizes of the computed quadratic electric response properties together with their type (octupolar/dipolar) are dominated by the BN patch. Let us now proceed with some crucial features about the respective polarization mechanism lying under the sizable computed hyperpolarizability values. For this task, we relied on the sum-overstates perturbative approach applied on *h*-$B_{12}N_{12}$−C_{114} putting also into the picture the hypothetical "parent dipoles" of *h*-$B_{12}N_{12}$−C_{222}. The results of this treatment, complemented by an analysis of the charge transfer process based on natural transition orbital (NTO),[37] are summarized in Figures 4 and 5.

We choose to begin with Figure 4, where four doubly degenerated charge transfer excited states belonging to *h*-$B_{12}N_{12}$−C_{114} together with the corresponding vertical excitation channels from (and to) the ground state are drawn. According to the configuration interaction singlets method (CIS), these states contribute the most to the hyperpolarizability lying along the *y*-axis (β_{yyy}). All three excitation paths implicate the lowest doubly degenerated low lying charge transfer state in the specific system, that is, state S_2. The low excitation energy and the large transition dipoles obtained at the CIS/6-31G(d) level correlate well with the sizable hyperpolarizability values predicted by analytic coupled perturbed Hartree−Fock (CPHF) and coupled perturbed Kohn−Sham (CPKS) computations. In addition, the spatial partitioning of the corresponding NTO pairs between the respective "empty hole" and the "excited particle" for the central charge transfer excitation $S_0 \rightarrow S_2$ implies that the dominant charge transfer process should involve electronic transitions engaging atoms forming the heterojunction between the *h*-BN and carbon atoms located at the peripheral graphene section. This picture also holds for the rest of the $S_0 \rightleftarrows S_n$ excitations with n = 28, 29, and 47.[38,39] In fact, all available indications suggest that the charge transfer process in the excited states should rely heavily on the particularities of the BN−graphene heterojunction with no significant contribution of the central nitroborazine ring.

The validity of the above analyzed charge transfer profile is further verified by disassembling these octupoles to their hypothetical independent dipolar units as shown in Figure 5 for *h*-$B_{12}N_{12}$−C_{222}. In the actual flake these fragments are merged together in a planar "core-shell-like" disk keeping at the same time an octupolar arrangement as substituting units of the octupolar $B_{12}N_{12}$ section. A careful inspection of all the intense charge transfer transitions found within the first 50 excited states of these "parent dipoles" computed within the time-dependent density functional framework using the Tamm−Dancoff approximation[40] and the CAM-B3LYP long-range corrected functional (TDA-CAM-UB3LYP) proves that the occurring charge transfer detains in each of the two substituting trigonal segments with no important charge transfer excitation paths between the two carbon wings through the BN segment. This is very well represented in the NTO pairs provided in Figure 5. As seen, a synergetic charge transfer occurs at each of the sides of these dipoles, independently. In the right wing charge migrates from the outer carbons rings to the $-C_3NB_2$ ring forming the heterojunction between the $B_{12}N_{12}$ and the graphene part. Apparently, in this case $-C_3NB_2$ ring acts as an electron acceptor pulling electronic charge form the neighboring carbon atoms. In the left wing the analogue $-C_3BN_2$ ring functions as an electron donor, pushing electronic charge to the outer carbons complementing in such a manner the occurring charge transfer in the right wing that is blocked by the $B_{12}N_{12}$ segment.

The presented results on the hypothetical parent dipoles of these species support the CIS picture discussed in the case of *h*-$B_{12}N_{12}$−C_{114} concerning the negligible implication of the central nitroborazine ring in the polarization mechanism being at the same time in accord with the nondelocalized nature of the BN section. This is nicely depicted at the bottom of Figure 5, where we show the FOHI 6-center π-bond delocalization indices (π-6-DIs), obtained through the QTAIM scheme implementation via the generalized population analysis (GPA) as shown by Mandado et al.[27] These indices directly represent the extent to which the electrons of a system are shared or delocalized among a set of n atoms with respect to the null Fermi hole-density. Increasingly positive DIs indicate increasing ring aromaticities (and thus delocalization), DIs close to zero are related to nonaromatic systems, while increasingly negative DI values imply antiaromatic molecular moieties. In our case the computed π-6-DIs clearly demonstrate the large differences in delocalization between the two carbon wings of the hypothetical parent dipole of *h*-$B_{12}N_{12}$−C_{222} and the central BN patch, with the latter being the less delocalized segment out of the three. This effect is caused principally by the large π-deficiency of boron, which removes a significant amount of nitrogen's electron density affecting the global delocalization on this part and, therefore, breaking the possible conjugation and aromaticity that could exist. As a result, no significant changes in hyperpolarizability should be expected after the central borazine ring of *h*-$B_{12}N_{12}$−C_{222} is removed. Indeed, the modulus $\|\beta\|$ of the unpassivated antidot structure counterpart of *h*-$B_{12}N_{12}$−C_{222} as computed at the CAM-B3LYP/6-31G(d) level of theory is found only 2% higher in magnitude than in *h*-$B_{12}N_{12}$−C_{222}. The small change observed in the computed first hyperpolarizability strengthens the picture delivered by the CIS outcomes concerning the small implication of the central borazine ring in the hyperpolarizability magnitudes of these systems. These outcomes verify very recent observations made by Yoneda et al.[41] about the negligible participation of the interior B and N atoms on the second hyperpolarizabilities of patched zigzag graphene flakes judging from the HOMO−LUMO energy differences and the shapes of molecular orbitals. However, in that work the observed oscillations in the second hyperpolarizability are attributed to changes in the diradical character of these species, a factor that is not connected to the systems studied here since at the levels of theory we applied, all systems bear closed shell singlet ground states of practically zero diradical character.

The revealed charge transfer mechanism allows for a better understanding of the intriguing hyperpolarizability evolution depicted in Figure 2 as a function of the position of the BN-patch. As shown in Figure 2 the maximum NLO response is delivered only when the BN patch is placed precisely at the center of the respective hexagonal arm-chair flake. As the BN

dx.doi.org/10.1021/ja502631w | J. Am. Chem. Soc. 2014, 136, 7464−7473

section moves closer to the flake-edges a dramatic hyperpolarizability decrease is experienced, which does not always correlate with the respective HL gaps as happens in conventional molecules. See for instance in Figure 2 that the original $B_{12}N_{12}-C_{222}-$(**#0**) hexagonal flake is characterized by wider HL gap (2.58 eV) than flakes **#1** (2.44 eV) and **#4** (2.41 eV) but larger and substantially larger quadratic NLO responses, respectively. Through the prism of the exposed synergic polarization mechanism, taking at the same time into account the hypothetical parent dipoles shown in Figure 5, this evolution seems now reasonable. More specifically, both the synergic electron-donating and -withdrawing functions of $-C_3BN_2/-C_3NB_2$ heterojunction rings of each parent dipole can be fully exploited at the same time only when the BN patch is placed precisely at the center of the graphene flake. On the other hand, when the BN section lies close to the flake edges, the ability of the $-C_3BN_2/-C_3NB_2$ rings, facing the flake borders, of pushing/pulling electrons upon excitation is hampered since they can set in motion "less valence electrons" than in the central position. As a result, the original flake **#0** is more hyperpolarizable than flake **#1**, which in turn proves more hyperpolarizable than flake **#4**. Note than in the last flake, which is the less hyperpolarizable out of the three, three out of six $-C_3BN_2/-C_3NB_2$ heterojunction rings are in fact put out of action because of their close proximity to the flake-edge. The same holds for flakes $B_{12}N_{12}-C_{222}-$**#3** and **#2**, which as the three previous ones bear HL gaps of more or less the same size. Flake **#3**, although bearing smaller HL gap than the latter, delivers weaker quadratic responses instead of stronger as one should have expected. Once again the more hyperpolarizable flake is the one in which the $-C_3B_2N$ $-C_3N_2B$ heterojunction rings of each parent dipole have access to more valence electrons of the neighboring benzene rings delivering intense charge transfer transitions. If the just described interpretation is correct, then, the quadric NLO response of the propeller-like graphene flakes shown in Figure 6, built from 150 heavy atoms should be smaller than the one obtained for $B_{12}N_{12}-C_{144}$ despite their larger size since in each propeller case three out of six heterojunction rings are precisely at flakes border. Indeed, CAM-B3LYP/6-31G(d) computations deliver $\|\beta\|$ values 3.1 and 3.5 times smaller than the one corresponding to $B_{12}N_{12}-C_{144}$ at the same level of theory.

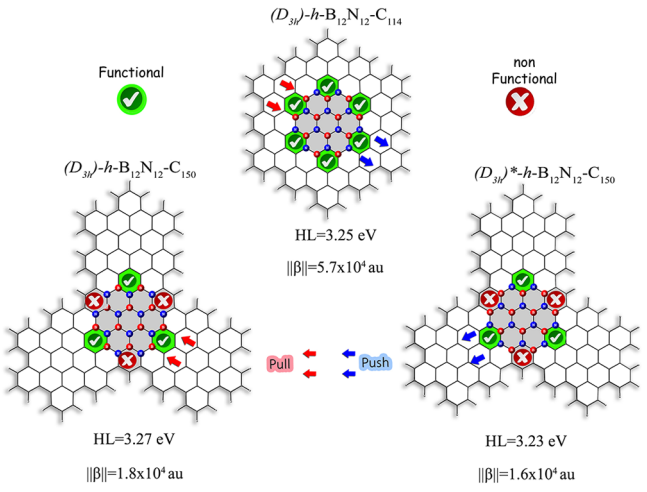

Figure 6. Hyperpolarizability comparisons among three *h*-$B_{12}N_{12}$/graphene flakes of different shapes and sizes but similar HOMO–LUMO (HL) gaps together with pictorial representation of the functional and nonfunctional $-C_3B_2N$ and $-C_3N_2B$ heterojunction rings of each BN patch as a function of their ability in setting in motion valence electrons belonging to neighboring benzene rings. All molecular properties have been computed at the CAM-B3LYP/6-31G(d) level of theory.

CONCLUSIONS

The current article demonstrates the large potential of hybrid *h*-B_nN_n–graphene finite sections in delivering systems of substantial quadratic NLO activities. State-of-the-art quantum chemical computations clearly suggest that white graphene islands embedded in graphene nanosheets may trigger large quadric NLO responses dominated not only by the sizes and global shapes of the hybrid flakes but also by the size, the position, and the shapes of the individual BN sections in their framework. More interestingly, this work points out the perspective of exploiting such graphene architectures in building NLO active species of exceptionally high octupolar quadratic NLO activities. As shown, even in systems with no classical octupolar shapes, large off-diagonal (β_{ijj}) tensorial hyperpolarizability components could be obtained by controlling the morphology and position of the embedded BN domains bringing in such a manner planar systems in which the NLO octupolar contributions reach or overshadow the dipolar ones. At the atomic level, CIS and time-dependent DFT computations predict that the prevailing polarization mechanism should involve mostly the heterojunction atoms of the B_nN_n sections and the graphene areas, whereas the contribution of the interior B, N atoms is most likely limited. The resolved nature of the charge transfer mechanism upon electronic excitation distinguishes these prototype graphene dipole/octupole motifs from other conventional pNA-like dipoles or TABT-type octupoles. In the latter class of dipolar/octupolar structural patterns the occurring charge transfer mechanism relies largely on the central units of the active molecules, whereas in the current case the peripheral graphene areas are those that play the most important role. We believe that the results presented in this article shall open up the subject of the quadric NLO properties of hybrid graphene systems stimulating more work toward the properties of these fascinating graphene-based hybrid motifs.

ASSOCIATED CONTENT

Supporting Information

Computational methods, basis set and electron correlation effects, definitions and more details about the fractional occupation Hirshfeld iterative (FOHI) method for the computation of atomic charges and 2- and 6-center delocalization indices. This material is available free of charge via the Internet at http://pubs.acs.org/.

AUTHOR INFORMATION

Corresponding Author

panagiotis.karamanis@univ-pau.fr

Notes

The authors declare no competing financial interest.

ACKNOWLEDGMENTS

This investigation is a part of the PICS project (No-6115). N.O. thanks CNRS for the one year post doc, and all authors thank Prof. Van Alsenoy for his kind help in computing the FOHI atomic charges needed for our discussion. This work was

granted access to the HPC resources of [CCRT/CINES/IDRIS] under the allocation 2013-2014 [No. i2013087031] made by GENCI (Grand Equipement National de Calcul Intensif). P.K. dedicates this work to Prof. G.M and Prof.'s wife A.M.

REFERENCES

(1) (a) Novoselov, K. S.; Geim, A. K.; Morozov, S. V.; Jiang, D.; Zhang, Y.; Dubonos, S. V.; Grigorieva, I. V.; Firsov, A. A.; Geim, A. K. *Science* **2004**, *306*, 666. (b) Novoselov, K. S. *Nat. Mater.* **2007**, *6*, 183.
(2) (a) Bonaccorso, F.; Sun, Z.; Hasan, T.; Ferrari, A. C. *Nat. Photonics* **2010**, *4*, 611. (b) Bao, Q.; Loh, K. P. *ACS Nano* **2012**, *6*, 3677−3694.
(3) Liu, Z.-B.; Zhao, X.; Zhang, X.-L.; Yan, X.-Q.; Wu, Y.-P.; Chen, Y.-S.; Tian, J.-G. *J. Phys. Chem. Lett.* **2011**, *2*, 1972−1977.
(4) Zheng, X.; Feng, M.; Zhan, H. *J. Mater. Chem. C* **2013**, *1*, 6759.
(5) Wang, J.; Hernandez, Y.; Lotya, M.; Coleman, J. N.; Blau, W. J. *Adv. Mater.* **2009**, *21*, 2430.
(6) Wu, R.; Zhang, Y.; Yan, S.; Bian, F.; Wang, W.; Bai, X.; Lu, X.; Zhao, J.; Wang, E. *Nano Lett.* **2011**, *11*, 5159 2011.
(7) Li, W.; Chen, B.; Meng, C.; Fang, W.; Xiao, Y.; Li, X.; Hu, Z.; Xu, Y.; Tong, L.; Wang, H.; Liu, W.; Bao, J.; Shen, Y. R. *Nano Lett.* **2014**, *14*, 955.
(8) (a) Avouris, P. *Nano Lett.* **2010**, *10*, 4285. (b) Gu, T.; Petrone, N.; McMillan, J. F.; van der Zande, A.; Yu, M.; Lo, G. Q.; Kwong, D. L.; Hone, J.; Wong, C. W. *Nat. Photonics* **2012**, *6*, 554−559.
(9) (a) Konishi, A.; Hirao, Y.; Matsumoto, K.; Kurata, H.; Kishi, R.; Shigeta, Y.; Nakano, M.; Tokunaga, K.; Kamada, K.; Kubo, T. *J. Am. Chem. Soc.* **2013**, *135*, 1430. (b) Yoneda, K.; Nakano, M.; Fukuda, K.; Champagne, B. *J. Phys. Chem. Lett.* **2012**, *3*, 3338−3342. (c) Yoneda, K.; Nakano, M.; Fukui, H.; Minami, T.; Shigeta, Y.; Kubo, T.; Botek, E.; Champagne, B. *ChemPhysChem* **2011**, *12*, 1697−1707. (d) Yoneda, K.; Nakano, M.; Inoue, Y.; Inui, T.; Fukuda, K.; Shigeta, Y.; Kubo, T.; Champagne, B. *J. Phys. Chem. C* **2012**, *116*, 17787.
(10) (a) Boyd, R. W. *Nonlinear Optics*; Academic Press: San Diego, CA, 1992. (b) Zyss, J., Ed.; *Molecular Nonlinear Optics: Materials, Physics and Devices*; Academic Press: New York, 1994. (c) Saleh, B. E. A. *Fundamentals of Photonics*; Wiley: New York, 1991.
(11) Kuzyk, M. G. *Circuits Devices Mag.* **2003**, *3*, 8755.
(12) Kanis, D. R.; Ratner, M. A.; Marks, T. J. *Chem. Rev.* **1994**, *94*, 195−242.
(13) (a) Yamuna, R.; Ramakrishnan, S.; Dhara, K.; Devi, R.; Kothurkar, N. K.; Kirubha, E.; Palanisamy, P. K. *J. Nanopart. Res.* **2013**, *15*, 1. (b) Thompson, J.; Crossley, A.; Nellist, P. D.; Nicolosi, V. *J. Mater. Chem.* **2012**, *22*, 23246. (c) Xu, Y.; Liu, Z.; Zhang, X.; Wang, Y.; Tian, J.; Huang, Y.; Ma, Y.; Zhang, X.; Chen, Y. *Adv. Mater.* **2009**, *21*, 1275. (d) Liu, Z.-B.; Xu, Y.-F.; Zhang, X.-Y.; Zhang, X.-L.; Chen, Y.-S.; Tian, J.-G. *J. Phys. Chem. B* **2009**, *113*, 9681. (e) Krishna, M. B. M.; Kumar, V. P.; Venkatramaiah, N.; Venkatesan, R.; Rao, D. N. *Appl. Phys. Lett.* **2011**, *98*, 081106.
(14) (a) Zhou, Z.-J.; Liu, Z.-B.; Li, Z.-R.; Huang, X.-R.; Sun, C.-C. *J. Phys. Chem. C* **2011**, *115*, 16282. (b) Ma, F.; Zhou, Z.-J.; Liu, Y.-T.; Zhang, Y.-Z.; Miao, T.-F.; Li, Z.-R. *Chem. Phys. Lett.* **2011**, *504*, 211. (c) Zhou, Z.-J.; Li, X.-P.; Ma, F.; Liu, Z.-B.; Li, Z.-R.; Huang, X.-R.; Sun, C.-C. *Chem.—Eur. J.* **2011**, *17*, 2414−2419.
(15) Karamanis, P.; Pouchan, C. *J. Phys. Chem. C* **2013**, *117*, 3134−3140.
(16) (a) Karamanis, P.; Otero, N.; Pouchan, C. *J. Mater. Chem. C* **2013**, *1*, 3035. (b) Karamanis, P.; Pouchan. *J. Phys. Chem. C* **2013**, *117*, 721−724.
(17) Zyss, J.; Ledoux, I. *Chem. Rev.* **1994**, *94*, 77−105.
(18) Ayhan, M. M.; Singh, A.; Hirel, C.; Gürek, A. G.; Ahsen, V.; Jeanneau, E.; Ledoux-Rak, I.; Zyss, J.; Andraud, C.; Bretonnière, Y. *J. Am. Chem. Soc.* **2012**, *134*, 3655.
(19) (a) Ci, L.; Song, L.; Jin, C.; Jariwala, D.; Wu, D.; Li, Y.; Srivastava, A.; Wang, Z. F.; Storr, K.; Balicas, L.; Liu, F.; Ajayan, P. M. *Nat. Mater.* **2010**, *9*, 430. (b) Krivanek, O. L.; Chisholm, M. F.; Nicolosi, V.; Pennycook, T. J.; Corbin, G. J.; Dellby, N.; Murfitt, M. F.; Own, C. S.; Szilagyi, Z. S.; Oxley, M. P.; Pantelides, S. T.; Pennycook, S. J. *Nature* **2010**, *464*, 571. (c) Levendorf, M. P.; Kim, C.-J.; Brown, L.; Huang, P. Y.; Havener, R. W.; Muller, D. A.; Park, J. *Nature* **2012**, *488*, 627. (d) Liu, Z.; Ma, L.; Shi, G.; Zhou, W.; Gong, Y.; Lei, S.; Yang, X.; Zhang, J.; Yu, J.; Hackenberg, K. P.; Babakhani, A.; Idrobo, J.-C.; Vajtai, R.; Lou, J.; Ajayan, P. M. *Nat. Nanotechnol.* **2013**, *8*, 119−124. (e) Gao, Y.; Zhang, Y.; Chen, P.; Li, Y.; Liu, M.; Gao, T.; Ma, D.; Chen, Y.; Cheng, Z.; Qiu, X.; Duan, W.; Liu, Z. *Nano Lett.* **2013**, *13*, 3439. (f) Kim, S. M.; Hsu, A.; Araujo, P. T.; Lee, Y.-H.; Palacios, T.; Dresselhaus, M.; Idrobo, J.-C.; Kim, K. K.; Kong, J. *Nano Lett.* **2013**, *13*, 933−941.
(20) (a) Zhao, R.; Wang, J.; Yang, M.; Liu, Z.; Liu, Z. *J. Phys. Chem. C* **2012**, *116*, 21098. (b) Shinde, P. P.; Kumar, V. *Phys. Rev. B: Condens. Matter Mater. Phys.* **2011**, *84*, 125401.
(21) Chang, C.-K.; Kataria, S.; Kuo, C.-C.; Ganguly, A.; Wang, B.-Y.; Hwang, J.-Y.; Huang, K.-J.; Yang, W.-H.; Wang, S.-B.; Chuang, C.-H.; Chen, M.; Huang, C.-I.; Pong, W.-F.; Song, K.-J.; Chang, S.-J.; Guo, J.-H.; Tai, Y.; Tsujimoto, M.; Isoda, S.; Chen, C.-W.; Chen, L.-C.; Chen, K.-H. *ACS Nano* **2013**, *7*, 1333.
(22) Bepete, G.; Voiry, D.; Chhowalla, M.; Chiguvare, Z.; Coville, N. J. *Nanoscale* **2013**, *5*, 6557.
(23) We considered rather armchair flakes than zigzag ones in order to avoid possible side effects of the disputable method performance in such systems (see ref 16a).
(24) Zhi, L.; Müllen, K. *J. Mater. Chem.* **2008**, *18*, 1472−1484.
(25) Bultinck, P.; Ayers, P. W.; Fias, S.; Tiels, K.; Alsenoy, C. V. *Chem. Phys. Lett.* **2007**, *444*, 205. Hirshfeld, F. L. *Theor. Chim. Acta* **1977**, *44*, 129.
(26) The delocalization indices were obtained following a QTAIM-based scheme implementation via the generalized population analysis (GPA) reported by Mandado et al. (see ref 27 and S.4 section of the Supporting Information).
(27) (a) Mandado, M.; González-Moa, M. J.; Mosquera, R. A. *J. Comput. Chem.* **2007**, *28*, 1625. (b) Mandado, M.; González-Moa, M. J.; Mosquera, R. A. *J. Comput. Chem.* **2007**, *28*, 127. (c) Otero, N.; González Moa, M. J.; Mandado, M.; Mosquera, R. A. *Chem. Phys. Lett.* **2006**, *428*, 249. (d) Otero, N.; M, J.; Mandado, M.; Mosquera. *Tettrahedron* **2006**, *62*, 12204.
(28) The task of defining whether the magnitude of a given electric response nonlinear optical property of a given system is large is not straightforward. As a result, most of the time final conclusions lie more on gained experience into the subject than on absolute criteria. Kanis and Ratner (see ref 12) attempted to establish some empirical limits concerning the magnitude of this property at a given optical frequency. This classification has been adopted also in theoretical studies carried out at static limit. Therefore, static first hyperpolarizability values ranging from 10^3 to 2×10^4 au are usually referred as "large", magnitudes between 2×10^4 and 10^5 au are usually considered as "very large". When the barrier of 10^5 au is outweighed, the hyperpolarizabilities are loosely described as "giant".
(29) Brunel, J.; Ledoux, I.; Zyss, J.; Blanchard-Desce, M. *Chem. Commun.* **2001**, *10*, 923.
(30) Brunel, J.; Mongin, O.; Jutand, A.; Ledoux, I.; Zyss, J.; Blanchard-Desce, M. *Chem. Mater.* **2003**, *15*, 4139.
(31) Brunel, J.; Jutand, A.; Ledoux, I.; Zyss, J.; Blanchard-Desce, M. *Synth. Met.* **2001**, *124*, 195−199.
(32) Going from *h*-$B_{12}N_{12}$−C_{84} to −C_{114} the modulus of the first hyperpolarizability increases by a factor of 5 at HF/6-31G(d) level and a factor varying from 7 to 9. Although the respective factor decreases to 3 or 4 depending on the level of theory used going from *h*-$B_{12}N_{12}$−C_{114} to −C_{222}, *h*-$B_{12}N_{12}$−C_{366} is still characterized by a $\|\beta\|$ value that is still about 2.5 times larger.
(33) Grimme, S. *J. Chem. Phys.* **2006**, *124*, 034108.
(34) Frisch, M. J.; Trucks, G. W.; Schlegel, H. B.; Scuseria, G. E.; Robb, M. A.; Cheeseman, J. R.; Scalmani, G.; Barone, V.; Mennucci, B.; Petersson, G. A.; Nakatsuji, H.; Caricato, M.; Li, X.; Hratchian, H. P.; Izmaylov, A. F.; Bloino, J.; Zheng, G.; Sonnenberg, J. L.; Hada, M.; Ehara, M.; Toyota, K.; Fukuda, R.; Hasegawa, J.; Ishida, M.; Nakajima, T.; Honda, Y.; Kitao, O.; Nakai, H.; Vreven, T.; Montgomery, J. A., Jr.;

Peralta, J. E.; Ogliaro, F.; Bearpark, M.; Heyd, J. J.; Brothers, E.; Kudin, K. N.; Staroverov, V. N.; Kobayashi, R.; Normand, J.; Raghavachari, K.; Rendell, A.; Burant, J. C.; Iyengar, S. S.; Tomasi, J.; Cossi, M.; Rega, N.; Millam, J. M.; Klene, M.; Knox, J. E.; Cross, J. B.; Bakken, V.; Adamo, C.; Jaramillo, J.; Gomperts, R.; Stratmann, R. E.; Yazyev, O.; Austin, A. J.; Cammi, R.; Pomelli, C.; Ochterski, J. W.; Martin, R. L.; Morokuma, K.; Zakrzewski, V. G.; Voth, G. A.; Salvador, P.; Dannenberg, J. J.; Dapprich, S.; Daniels, A. D.; Ö. Farkas, Foresman, J. B.; Ortiz, J. V.; Cioslowski, J.; Fox, D. J. *Gaussian 09*, Revision C.01 and D.01; Gaussian, Inc.: Wallingford, CT, 2009.

(35) Maroulis, G. *J. Chem. Phys.* **1998**, *108*, 5432. Maroulis, G. *J. Chem. Phys.* **2003**, *118*, 2673−2687. Karamanis, P.; Maroulis, G. *Chem. Phys. Lett.* **2003**, *376*, 403.

(36) Each pristine graphene flake shown in Figure 3 belongs to the D_{2h} symmetry point group. After a D_{3h} patch is incorporated in the center, a system of C_{2v} symmetry is delivered. On the other hand, when finite BN sections of C_s symmetry are chosen, the arising *h*-BN−graphene hybrid systems adopt the latter symmetry constrains.

(37) Martin, R. L. *J. Chem. Phys.* **2003**, *125*, 4775.

(38) The same results are obtained at the TDA-UCAM-B3LYP/6-31G(d) level of theory (see ref 39).

(39) Trani, F.; Scalmani, G.; Zheng, G. S.; Carnimeo, I.; Frisch, M. J.; Barone, V. *J. Chem. Theory Comput.* **2011**, *7*, 3304.

(40) Hirata, S.; Head-Gordon, M. *Chem. Phys. Lett.* **1999**, *314*, 291.

(41) Yoneda, K.; Matsui, H.; Fukuda, K.; Takamuku, S.; Kishi, R.; Nakano, M. *Chem. Phys. Lett.* **2014**, *595*−*596*, 220.